AD-A264 687

1. AGENCY USE ONLY (Leave blank)	2. REPORT DATE	3. REPORT TYPE AND DATES COVERED
	March 1993	Professional Paper

4. TITLE AND SUBTITLE

UPLINK LASER PROPAGATION MEASUREMENTS THROUGH THE SEA SURFACE, HAZE AND CLOUDS

5. FUNDING NUMBERS

PR: CM98
PE: 0303901N
WU: DN301057

6. AUTHOR(S)

G. T. Kaye, R. Nies, M. Lovern

7. PERFORMING ORGANIZATION NAME(S) AND ADDRESS(ES)

Naval Command, Control and Ocean Surveillance Center (NCCOSC)
RDT&E Division
San Diego, CA 92152–5001

8. PERFORMING ORGANIZATION REPORT NUMBER

9. SPONSORING/MONITORING AGENCY NAME(S) AND ADDRESS(ES)

Naval Intelligence Command
Joint Nation Intelligence Development Staff
Suitland, MD

10. SPONSORING/MONITORING AGENCY REPORT NUMBER

11. SUPPLEMENTARY NOTES

12a. DISTRIBUTION/AVAILABILITY STATEMENT

Approved for public release; distribution is unlimited.

12b. DISTRIBUTION CODE

13. ABSTRACT (Maximum 200 words)

An Airborne Optical Receiver (AOR) was developed and tested to investigate the propagation and reception of optical communications uplinks from a submerged laser source to an overflying fleet aircraft. The AOR was flown in a P-3C Orion aircraft for an at-sea test off the southern California coast in August, 1990. A green laser transmitter was suspended from the Research Platform FLIP at depths of 15 to 45 m. During six nights of operations, the AOR received the laser light at various test geometries and through clear and cloudy conditions.

This represents the first optical uplink cloud experiment at visible wavelengths. Results show that optical pulses in clouds are significantly more forward-scattered than modeled. The results can be explained by Mie scattering theory. Measured cloud attenuation and pulse stretching agreed with an existing optical propagation model. Signficant attenuation and signal spreading due to haze and fog was measured and compared with theory.

93 5 3

93-11363

~~Published in *SPIE Proceedings*, Vol. 1479, 23 Jul 1992, pp 162–173.~~

14. SUBJECT TERMS	15. NUMBER OF PAGES
lasers air-based optical radiation detection	16. PRICE CODE

17. SECURITY CLASSIFICATION OF REPORT	18. SECURITY CLASSIFICATION OF THIS PAGE	19. SECURITY CLASSIFICATION OF ABSTRACT	20. LIMITATION OF ABSTRACT
UNCLASSIFIED	UNCLASSIFIED	UNCLASSIFIED	SAME AS REPORT

21a NAME OF RESPONSIBLE INDIVIDUAL	21b TELEPHONE (Include Area Code)	21c OFFICE SYMBOL
G. T. Kaye	(619) 553-2109	Code 731

Uplink Laser Propagation Measurements Through the Sea Surface, Haze and Clouds

G. Thomas Kaye, Roger Nies and Michael Lovern
Research, Development, Test and Evaluation Division
Naval Command, Control, and Ocean Surveillance Center
San Diego, California 92152-5000

ABSTRACT

An Airborne Optical Receiver (AOR) was developed and tested to investigate the propagation and reception of optical communications uplinks from a submerged laser source to an overflying fleet aircraft. The AOR was flown in a P-3C Orion aircraft for an at-sea test off the southern California coast in August, 1990. A green laser transmitter was suspended from the Research Platform FLIP at depths of 15 to 45 m. During six nights of operations, the AOR received the laser light at various test geometries and through clear and cloudy conditions.

This represents the first optical uplink cloud experiment at visible wavelengths. Results show that optical pulses in clouds are significantly more forward-scattered than modeled. The results can be explained by Mie scattering theory. Measured cloud attenuation and pulse stretching agreed with an existing optical propagation model. Significant attenuation and signal spreading due to haze and fog was measured and compared with theory.

1. INTRODUCTION

The Airborne Optical Receiver (AOR) was designed as an uplink comunications receiver to be operated in a P-3C Orion aircraft and was developed for the Navy by GTE-Mountainview. Research objectives were to: (1) verify AOR design parameters through laboratory calibration; (2) demonstrate the field ability to acquire and track laser emissions; and (3) characterize radiance profiles for a submerged laser propagating through water and clouds.

The AOR is a quadrant tracking sensor with signal processing primarily designed for a communications receiver. It has a 25-cm diameter optical aperture. Optically it performs from optical light levels of full nighttime to 10% of full sunlight. It was required to receive four femto-joule signal pulses of up to five microseconds widths against a background of 175 watts/m^2/micron, with a 20 dB Signal-to-Noise Ratio (SNR) at wavelengths between 530.0 and 532.5 nm. The receiver uses a narrowband optical filter, based upon Cadmium Sulfide (CdS) technology and is temperature-tuned. After filtering, the signal photons are detected by four photomultiplier tubes, whose outputs are then used as a quadrant tracker to maintain the receiver's view upon the laser signal source. Mechanically, since it is an airborne device, it has a lateral (side-to-side) scanning capability, as well as fore-and-aft scanning. The receiver can change from a scanning to a tracking mode after acquisition of the laser signal.

2. EXPERIMENTAL DESIGN

The field test was designed to provide airborne measurements of subsurface, upwelling, pulsed laser signals under a variety of field environmental conditions. The test site was centered at 31° 12' N, 119° 41' W, a location about 275 km west-southwest of San Diego. The laser source was suspended at various selected depths from a boom on the Research Platform FLIP of the Marine Physical Laboratory of Scripps Institution of Oceanography. This is a 90-m surface vessel, which flips into a vertical spar buoy configuration. FLIP's stability also allowed for numerous complementary environmental measurements to be made at the sea surface. The uplink laser was from Martin-Marietta Corporation of Baltimore. This device proved to be a rugged and reliable laser that consistently delivered 15 millijoules of pulse peak energy within the receiver band near 532 nm. The AOR was flown in a Navy P-3C Orion aircraft operated by Naval Air Warfare Center - Aircraft Division -Warminster. It was mounted in the belly of the fuselage with downward viewing through a large, plexiglass window. The AOR has a lateral scanning capability for searching and a fore/aft tracking capability to maintain view of the laser signal after acquiring the uplink beam.

Uplink propagation was measured during a geometrically-varying series of runs to define the angular signal distribution. Altitude and offset variations from run to run depended upon transmitter depth, clouds and water type. Variations were planned in real time during the test to adjust to specific conditions. A second sampling approach provided for a straight and level pass through the laser beam, with the AOR looking straight down at nadir, in order to make radiance measurements of the spot size coming out of the cloud tops. This scenario was also flown at altitudes of 150 m to make measurements of the spot coming out of the water surface.

2.1 Airborne Optical Measurements

Six data-taking flights were flown from 30 July to 7 August, 1990. The majority of the scientifically-useful data were obtained on three sorties. Optical measurements during the sorties focused on various technical objectives. This resulted in different experimental geometries among and within sorties, some of which are depicted in figure 1. The typical laser depth was 30 m, varying from 15-45 m during the experiment. Cloud base altitudes were consistently around 300 m; cloud thicknesses were around 300 m. Offsets ranged from zero (overhead pass) to less than 9 km from the FLIP. Expected spot sizes on the water were tens of meters and for the cloud top spots, hundreds of meters. The AOR Field Of View (FOV) range was usually 10° for most runs.

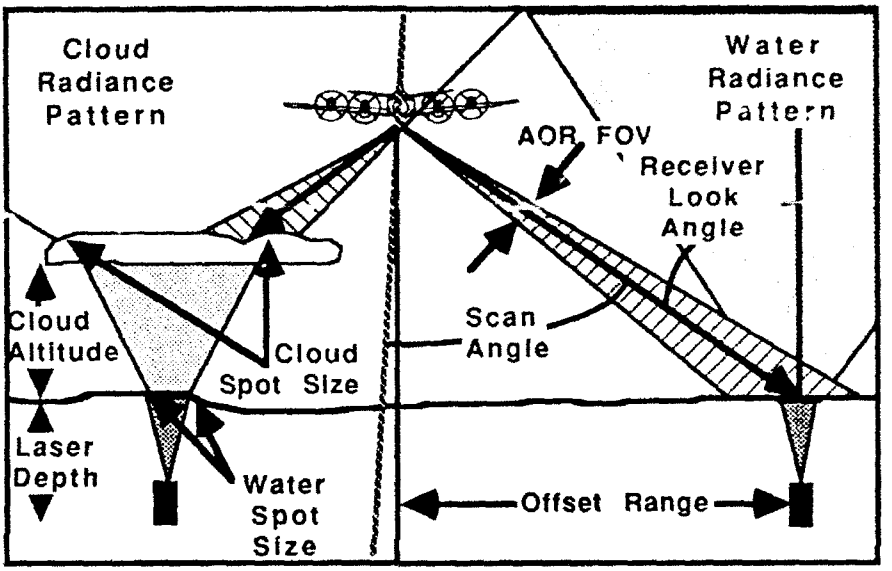

Figure 1. Experiment geometry for propagation measurements.

Receiver look angle and scan angle are different. Look angle is measured from the laser spot center to AOR and is measured in the earth's three-dimensional frame of reference with respect to nadir. Scan angle is measured from the normal to the aircraft fuselage to laser spot with respect to the aircraft's frame of reference. The aircraft's motion requires monitoring of aircraft pitch, roll and yaw to calculate receiver look angle.

2.2 Environmental Measurements

Near-surface profiles of water temperature and optical attenuation were measured. The temperature profile had a well-developed wind-mixed layer which extended from the surface to depths around 37 m, which covered most of the uplink laser transmitter depths during the test. Below this depth the diurnal thermocline began with a rapid temperature decrease from 18° to 10° by the 100 m depth. The upper ocean diffuse attenuation coefficients, integrated from the surface to 37 m, ranged from 0.075 to 0.087, in units of inverse meters. Sea surface wave height time histories were measured and recorded with three separated wave wires. During the experiment, seas remained nearly calm with small westerly swells. Thus surface wave scattering of the uplink beam was minimal and within the optical measurement errors. No further surface wave analysis was performed. Winds during the test remained very light at 5 m/sec or less for the entire duration and were consistently from the west.

Clouds were typical southern California marine stratus clouds with bases generally at 300 m altitude and physical thicknessess around 300 m. Optical thicknesses ranged from no clouds to a maximum optical thickness, τ, of 28. During daylight the optical thickness was determined by measuring the downwelling solar irradiance at the FLIP. A sling psychrometer and an adiabatic lapse rate were used to estimate cloud base heights. After nightfall physical thickness and cloud base height were measured directly by the aircraft, as it descended from transit altitude to the site location. Clouds generally thickened during the night as the marine layer moved toward the coast. Optical thickness was inferred from the laser pulse stretching observed in the received pulse width data. All of the data sorties had received pulse widths of 1.3-1.8 μsec and the pulse width data were well-behaved with only small pulse-to-pulse variation in received pulse width.

3. DATA PREPARATION

Figure 2 shows pulse energy data for a typical run. The aircraft was flying toward the source and scanning ahead (positive look angles) when detection was made and tracking began. The majority of the sampled data were taken after the aircraft had passed its closest point of approach and was tracking behind (negative look angles). This information, combined with a point-by-point knowledge of the source-receiver geometry, as well as the aircraft's attitude, allows the mapping of the data conformally into a plot of pulse energy as a function of look angle.

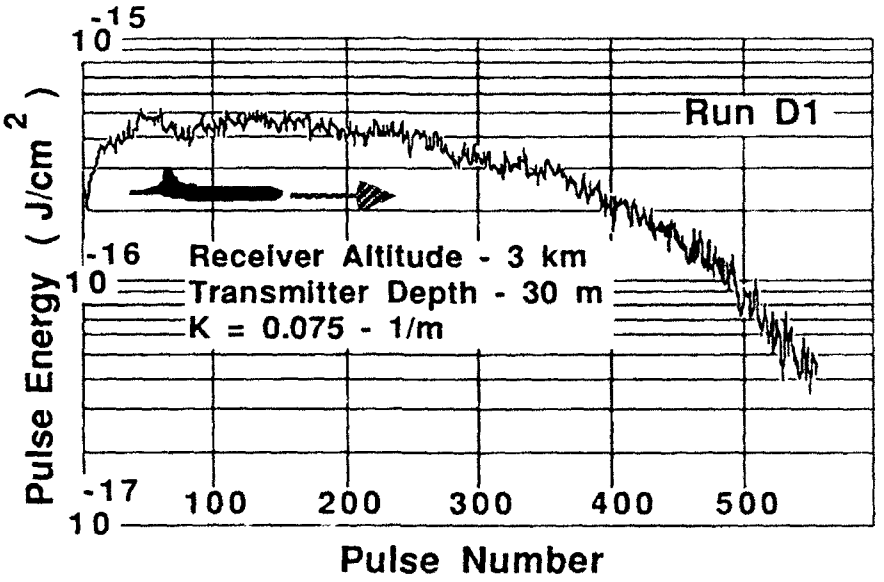

Figure 2. Raw optical energy data.

For each point, the aircraft's three-dimensional attitude, its course, and absolute positions of laser and receiver were combined to calculate the receiver look angle relative to the uplinking source. Since the laser was modulated at a straight 10 Hz repetition rate, it was fairly simple to sort signal pulses from noise. The level on each signal pulse was checked to ensure that AOR was not in saturation. If saturated, the point was deleted. Similarly the noise value for each sample was checked relative to the signal level to ensure sufficient SNR.

The remaining data were considered valid samples for analysis. Propagation loss was estimated for each point based upon the physical geometry between source and receiver. All pulses were normalized to the same distance by assuming spherical signal spreading from the source to the receiver. The distance-normalized data are well-behaved in the sense that there are no wild fluctuations in adjacent data points. Rather fluctuations of less than 5% in energy level from point to point are typical. As signal level decreases, this fluctuation increases until the AOR loses track on the laser.

A data-averaging process was used in order to provide regularly-spaced samples in look angle space. All samples were sorted according to look angle into 1° bins of look angle, +/-0.5° of bin center. After sorting, the samples in each bin were averaged linearly and the single value was used to represent the bin. Sample sizes typically ranged from five to ten samples per bin of look angle. Because the data were well-behaved for the majority of the runs, it was decided that a linear average, rather than a weighted average of sample values like a root-mean-square approach, presented a truer representation of the information.

Similar to the pulse energy data, a plot of the received pulse widths showed minimal pulse-to-pulse variability. Most pulses for this run suffered a minimal stretching of 1.5 μsec in their widths, as they propagated through the stratus clouds off San Diego. All of the pulse widths ranged between 1.0 and 2.0 μsec and 95% of the widths were between 1.3 and 1.7 μsec. Given that these clouds are fairly-homogenous marine stratus clouds, great pulse-to-pulse variability was not expected. The greatest pulse-to-pulse fluctuation was found at the higher look angles, where the optical SNR was rapidly falling off. These data proved valuable in understanding changes in optical thickness of clouds during the sortie.

4. ANALYSIS RESULTS

4.1 Haze Propagation

Data were gathered on six separate aircraft sorties, labeled A through F. Sortie F was the only time when there were no clouds and data from this sortie are in figure 3. AOR tracked the uplink spot as source-receiver geometry ranged over look angle space. Positive look angle data were usually taken during signal acquisition and prior to laser tracking. Most scientifically useful data were taken at negative look angles, after AOR was stable in its tracking. Only one run, F4, occurred in completely non-cloudy conditions, but haze was clearly visible to observers during this run. The haze radiance profile is exponentially-shaped and is attenuated by 10 dB from standard clear conditions. This profile can be described very well by an simple exponential function of look angle, θ, with a 1/e change in signal energy for a 21° change in look angle. Eo is the received pulse energy at 0° look angle. This exponential function is plotted and agrees with the data to within a few per cent over most all look angles. This is the first detailed field measurement of this function over a wide range of nearly continuous look angles.

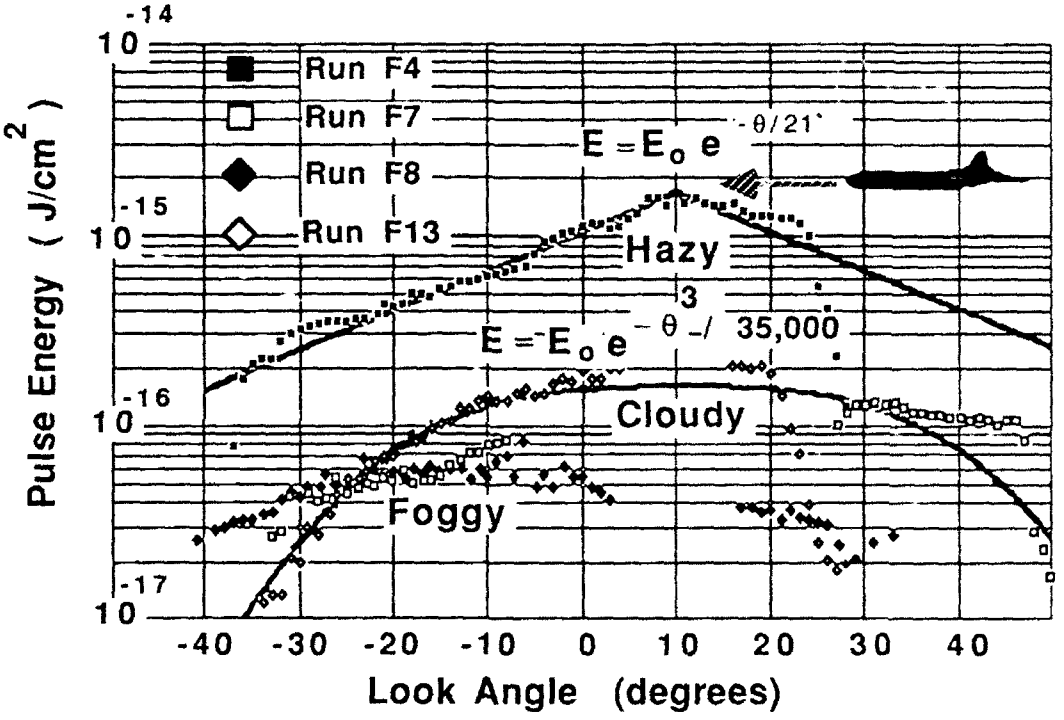

Figure 3. Sortie F radiance results.

By Runs F7 and F8, conditions were transitioning from hazy to foggy. The foggy radiance profiles are also exponentially-shaped and are attenuated by an additional 5 dB over Run F4. Received pulse energy decreased an order of magnitude from Run F4 to subsequent runs, even though the laser was raised from 38 m in Run F4 up to 30 m for later runs. A 2 dB (58 %) increase in signal level had been expected rather than a large decrease. The cloudy radiance profile of Run F13 is shaped like a cubic of an exponential and is less attenuated at small angles than the foggy runs. This suggests that much of the fog dissipated as the clouds formed over the experimental site.

There are few previously measured radiance profiles to provide experimental insight. A cosine function was used to model the profiles for ease of implementation. The measured peak energy density of 1.5 E-15 J/cm^2 was an order of magnitude weaker than modeled for observed propagation conditions and remained low at all look angles. Reexamination of the data revealed a severe underestimate of marine haze effects upon optical attenuation at visible wavelengths. Although the modeled visibility value was 23.5 km, a "standard clear" condition, the received energy required visibilities of 1-2 km, heavy haze to thin fog, to attenuate the signal to measured levels. Relative humidity was estimated on FLIP with a sling psychrometer. On the day before this night test, humidities ranged from 75% to of 81% at two hours prior to the sortie runs. Hazes exist at relative humidities less than 80%; light fogs form at humidities above 80%. This suggests that the optical data were taken in conditions of haze to light fog.

Figure 4 compares measurements to the continental haze model of Deirmendjian[1]. Bin-averaged data are plotted as discrete points. Two model predictions show the range of values for visible and infrared wavelengths. The exponential data fit is plotted and a clear air model prediction. The haze model and the measurements agree closely in received level, as well as in curve shape. The haze model has a curve slope with increasing look angle that is slightly steeper than measured results. Using Deirmendjian marine haze models resulted in even steeper curve slopes with increasing look angle. Other models which use wind speed and humidity could have been investigated.

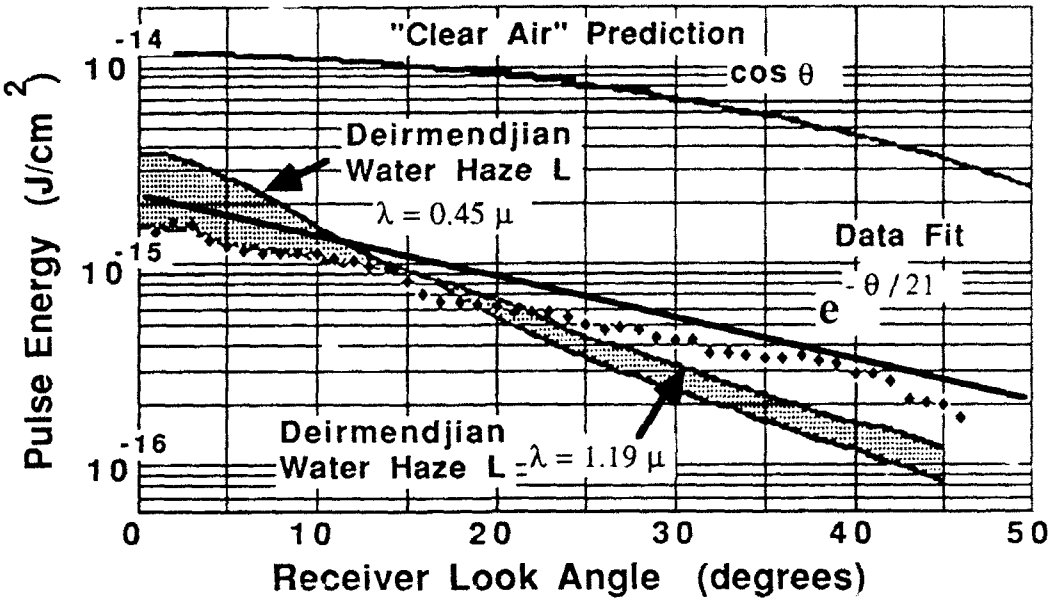

Figure 4. Comparison of measurement with haze model.

The Mie scattering parameter is the ratio of the size of the "typical" particle radius (times π) to the optical signal wavelength. When it is greater than unity, Mie scattering theory is generally used to describe the process. Figure 5 compares the measured data with a calculated distribution from Karp.et.al.[2] for a Mie scattering parameter of 8.5, which would be a typical particle radius of 1.4 μ for a 532 nm wavelength. This radius is very close to typical particle sizes measured in marine fogs off San Diego and the California coast[2]. The calculated phase function agrees with the measured data in the upper left-hand corner and both are plotted on the same scale sizes.

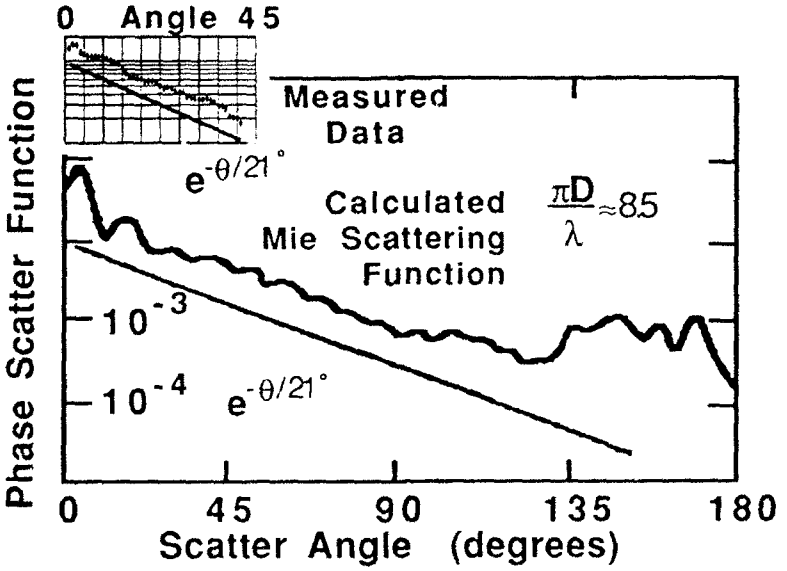

Figure 5. Comparison of measurement with a Mie scattering function.

Three results are apparent in this comparison. First, the use of a simple exponential expression to describe both the Mie scattering function and the measured data is reasonable for scatter angles of 0-90°. Certainly if uncertainties of around +/-1 dB in the uplink modeling are acceptable, the use of an exponential function for the haze radiance profile for these angles is acceptable and accurate. Second, the fine structure in the measured data, the small-scale variations with look angle changes of 10-30°, may be real variations in the scatter function and not simply noise in the measurement. The 1° resolution used for the bin-averaging process was too coarse to test this hypothesis. The raw data would have to be re-binned into sub-degree resolution elements; however, this could be done. Additional modeling work would be required to prove, or disprove, this point. Third, there is no high-energy forward scattering peak at very small angles. Many models for visible wavelengths suggest that at angles less than 5°, there is a "hot spot" of strong forward scattering, followed by a rapid fall-off for look angles greater than 5°. Measurements of this radiance profile were done down to a minimal look angle of 2°. If a hot spot in the profile does exist in nature, it should have been apparent in the data. It was not.

This strongly suggests that the water radiance profile was masked by haze or fog during those times when clouds were not present. The water radiance pattern was probably not actually measured. Past sea tests probably also provide few measurements of the water radiance profile for two reasons. First, previous receivers had insufficient dynamic range and lacked the automated tracking and navigation capability from airborne platforms needed to sample the radiance profile over a wide range of look angles. Second, most past experiments have been conducted off San Diego during summer nights, when hazy conditions should be expected.

The best data were taken on several runs of the LAMBDA experiment during summer nighttime conditions off San Diego[3]. For this test, a simple helicopter-mounted receiver was manually trained on the uplink spot from a submerged lamp. Data sets from the two best runs, consisting of 11 discrete measurements which spanned more than 20° of look angle, are plotted in Figure 6. Also plotted are a cosine-squared power model curve and two least-squares fits for exponential curves passed through the discrete points from both runs. Data were not taken at small look angles because the receiver went into saturation. The exponentials clearly fit the data as well as the cosine function. Both runs had 1/e fall-off points around the 21° value measured during the AOR test. This is true even though the runs were at different scattering distances into the fluid. The observers noted the visual occurrence of a heavy haze and they were unable to account for the propagated energy in a link budget. The curve shape plus the missing energy suggests that these were also measurements of a haze radiance rather than the water radiance profile.

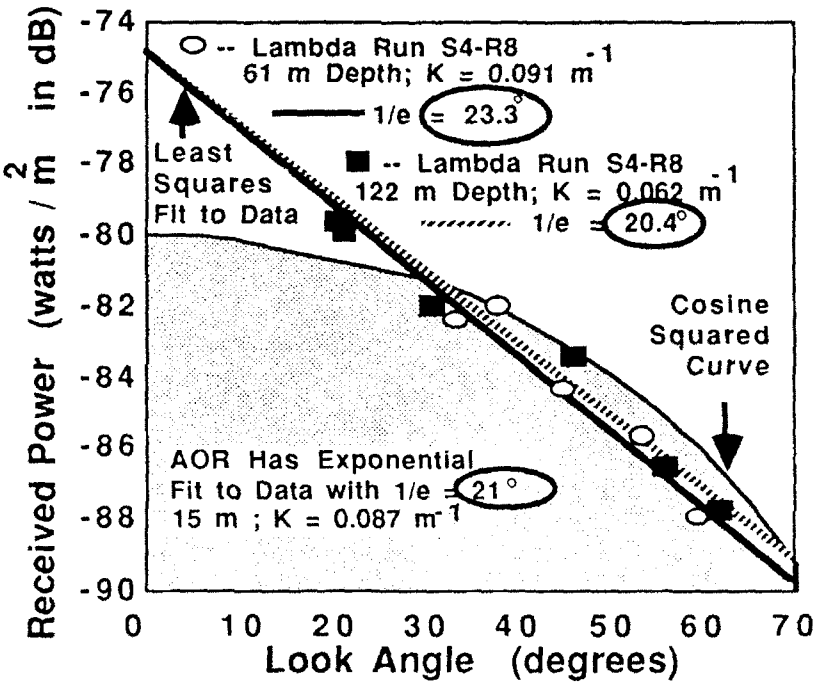

Figure 6. Water radiance profile data from LAMBDA experiment.

4.2 Cloud Spot Energy Distributions

During the sortie, two runs were used to measure laser beam spot characteristics on cloud tops. AOR was fixed in a staring orientation, 4.5° forward, as the aircraft was piloted over the laser spot at the cloud top. Results of the two runs are plotted in the figure 7. Propagation conditions were the same for both runs, but the FOV was expanded from 5° for the first run (lower curve) to 10° for the second run (upper curve). So, in the second run, more energy was allowed into the AOR for detection.

Both data plots can be closely approximated by the Gaussian distribution listed in the figure, with spot energy falling off by a factor of 1/e in a distance of 365 m. The small unfilled squares in the plot are discrete calculations for a Gaussian distribution and fit the measurements very well. The half-energy distance, an important parameter for estimating cloud spreading losses, is calculated as 305 m from this expression. Thus the calculated distance is very close to the half-energy distances actually measured. A standard rule of thumb is that spot size scales with cloud thickness and this agrees within measurement error for these runs.

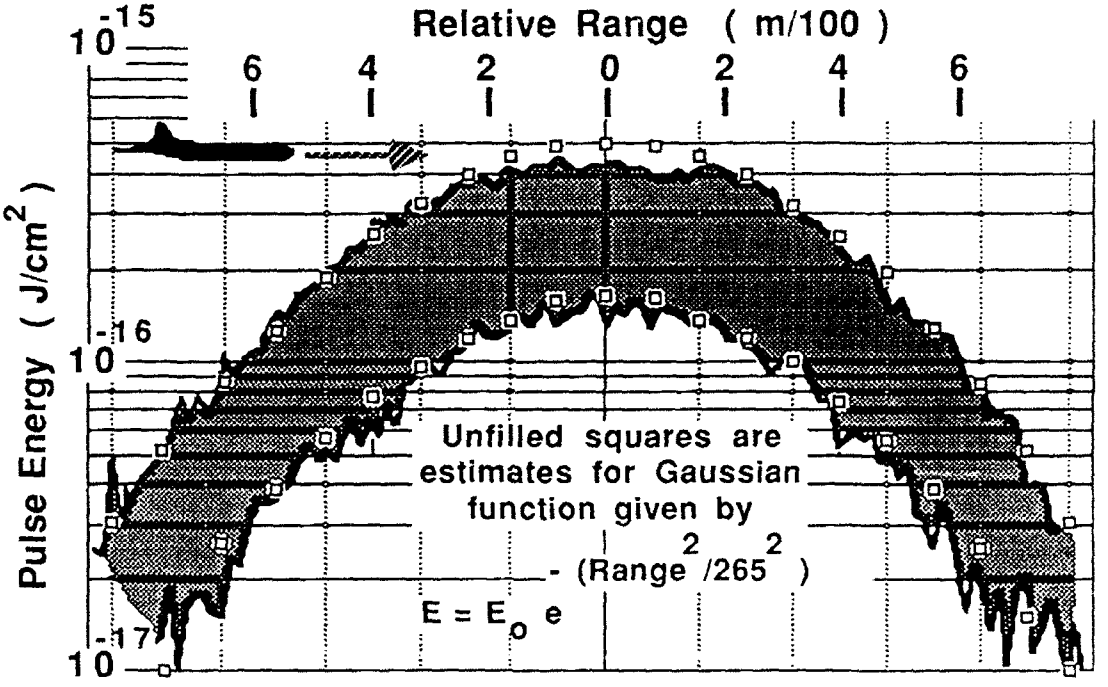

Figure 7. Cloud spot energy distribution.

Our current model estimates cloud spreading based upon a data optimization of measured solar irradiance through cloud cover, since the cloud spreading process does not lend itself to analytical solution[4]. This approach sorts clouds into two cases: optically thin and optically thick. The boundary between the two conditions is estimated to occur at an optical thickness value, τ, of 10. Cloud conditions for the experiment were not within the conditions specified for the modeling optimization. This is due primarily to the specialized conditions of California marine stratus clouds, which was discussed by Deirmendjian[2]. The observed clouds had sufficient optical thickness (τ =26) for use of the model, but the cloud base was too low (300 m) and the cloud's physical thickness (300 m) was too thin to be within the stated boudary conditions of the model.

The spot radius on the cloud top is calculated by the model for both cases. The model's optically thin case estimates a spot radius of 260 m, while the thick case estimate is 130 m. Both estimates are significantly less than the measured radius of 1000 m. Because of this, cloud spreading losses are underestimated by the ratio of measured and calculated spot sizes. The size of the underestimate is 20 Log (130 m / 305 m) = -7.3 dB. The peak measured value for the top curve of the figure is equal to 4.2 E-16 J/sq cm, while the model estimates a value of 1.95 E-15 J/sq cm for experimental conditions. So the measurement is about 6.7 dB less than prediction. Applying the cloud spreading correction yields a final ratio of -0.6 dB between measured and modeled received laser energy.

4.3 Cloud Propagation

Data from seven runs of Sortie D are plotted in figure 8, all for an aircraft altitude of 5000 m. The laser was at a depth of 30 m for earlier runs and lowered to 45 m by run D5. Cloud conditions were measured two hours prior to the start of data-taking for Run D1. The cloud base was at an altitude of 400 m with a layer thickness around 600 m and the clouds had an optical thickness around 20 at the start. The last cloud measurement occurred during the sortie before Run D5. The base of the clouds had lowered to an altitude of 300 m and thickness had decreased slightly to 500 m. As the clouds physically thinned slightly, the optical thickness of the cloud layer had increased from 20 to a value of 28. After this, nighttime conditions precluded further direct cloud measurements. The exponential curves fitted through the data are identical in form to that shown earlier for Run F13 in Figure 3. Pulse energies decreased monotonically about an order of magnitude with increasing run number during the sortie. This was true for most all look angle information as well. The confusion in the data at positive look angles near 30° is due to an artifact of the signal acquisition process.

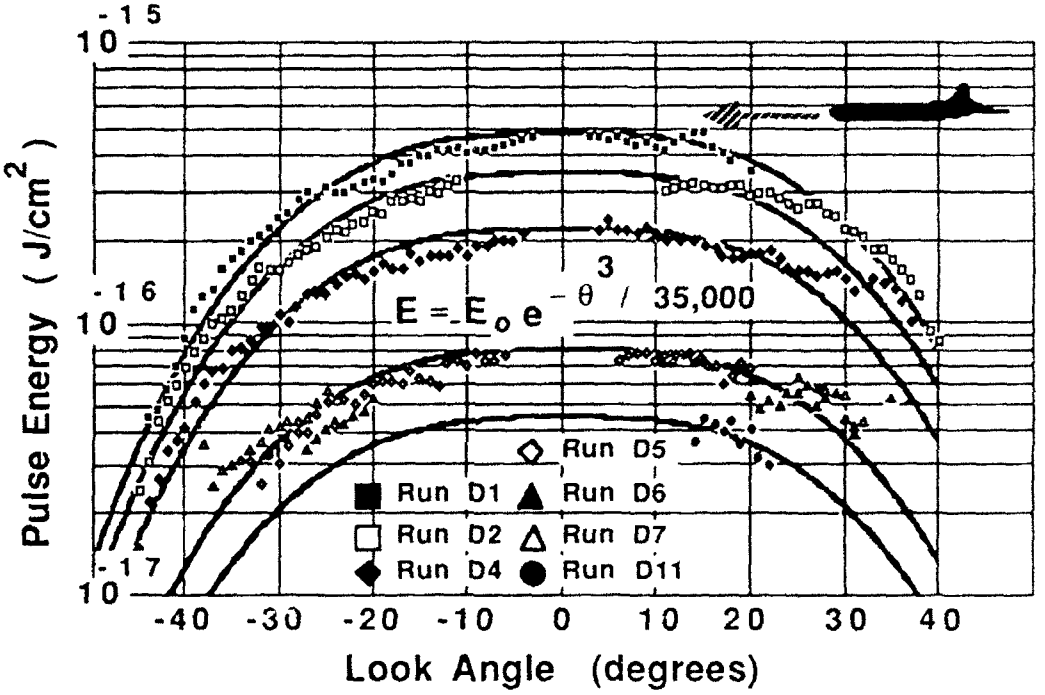

Figure 8. Sortie D cloud radiance results.

The changes in cloud thickness, cloud height and optical thickness seem too small to account for the large-scale decreases in received energy during the sortie. Each of these factors was investigated to determine if any factor or a combination could explain the decrease. Changes in cloud base altitude were investigated parametrically and produced very small effects. Measured pulse widths for the runs generally increased from an initial value of 1.5 μsec for Run D1 to 1.9 μsec for Run D11. This increased pulse stretching also has little effect on received energy.

The only remaining factor is the meteorological visibility during the sortie. As previously mentioned, our default model value for visibility is "standard clear", or a range of 23.5 km. However, for the "clear" run in Sortie F, the measured relative humidity indicated that conditions were actually those of a haze or light fog. This visibility difference led to readjustment of atmospheric attenuation losses needed to reach agreement between modeling predictions and actual received energies. The relationship between SNR and meteorological visibility for Sortie D conditions is plotted in Figure 9. During times of either clear or standard clear conditions (>15 km), there is very little impact upon SNR because of atmospheric visibility. However, for hazy conditions, a decrease in visibility of several kilometers can attenuate received energy by up to 5 dB. As conditions transition from haze to fog, energy attenuations of several dB come with visibility decreases of tenths of kilometers. Indeed, the differences among the runs of Sortie D are best explained by using a medium haze of 5.5 km visibility for Run D1, which degrades to a haze of 3.8 km visibility for the later runs. It is an apparently small change with a major impact. This again points to the need for visibility measurements in optical propagation experiments in order to understand the observations.

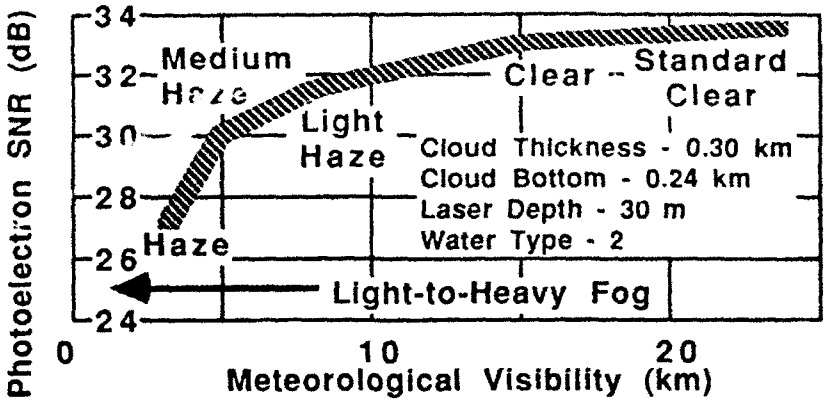

Figure 9. SNR vs. meteorological visibility.

The other major observation from the Sortie D data is the similarity, for all runs, of the curve shapes for pulse energy versus look angle. Our uplink model uses a cosine function to describe the radiance pattern out of cloud tops. For a cosine radiance profile, the half-energy value occurs at a 60° look angle and energy reaches 10% of its peak value at a look angle of 84°. All of the measured data clearly drop off much more quickly with look angle than a cosine function. The half-energy level is reached by a look angle of 29° and energy falls to less than 10% of peak value by a look angle of 45°. Peak values at 0° look angle vary due to changes in atmospheric visibility.

All data curves are fitted very well by the exponential expression shown in the figure. A cubic expression for look angle in the exponential was chosen after attempting numerous quadratic fits to the data. Closer observation of these data fits shows that the curves fall off slightly faster than the data. A smaller power around 2.9, rather then 3.0, would fit better. However, using a single expression for all rather than a unique profile for each was preferred. The reasonable fit of this expression for every cloud radiance run of Sorties D, E and F demonstrates its generality.

Figure 10 shows the seven data runs of Sortie E. Physical cloud conditions were similar to the latter part of Sortie D. The cloud base was at an altitude near 300 m and the cloud layer was 500 m thick. Unlike Sortie D final conditions, the optical thickness for Sortie E was much thinner with a value of 18. The laser was at a depth of 30 m. The aircraft altitude of 3 km for these runs was much lower than the 5 km of Sortie D. This changes the experiment geometry relative to the clouds, but had only minimal impact on the propagation results.

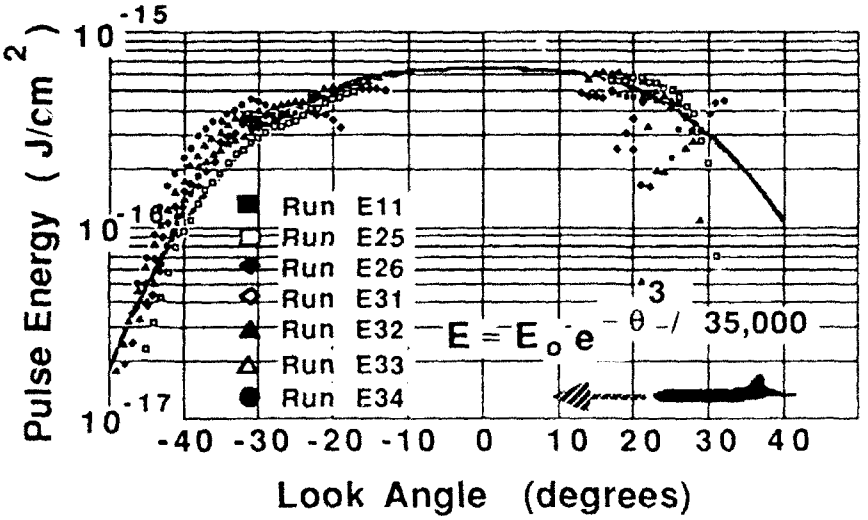

Figure 10. Sortie E cloud radiance results.

The absolute energy values from these seven runs plot nearly on top of one another for smaller look angles. Typical peak energy values around 5E-16 J/sq cm were observed for many Sortie E runs. At larger look angles (>35°), the data from different runs spread over an energy range of a factor of four (5-6 dB). Received pulse energy tends to increase during the sortie. The reason for this increase is that the visibility conditions for Sortie E were significantly different than those for Sortie D. A light haze is estimated for the early runs, with visibility improving to clear conditions, or better, for the later runs. There was no significant change in pulse width as a function of run number. Most runs were 1.3 in average with another run at 1.4 and one at 1.5.

Again these data fall off more quickly than a cosine function for describing the cloud radiance pattern and energy values fall off to 10% of peak value by a look angle of 45°. Again the data are well-described by the same exponential expression of the cube of the look angle. Unlike Sortie D, the data fall off slightly faster than the expression. Optimizing the fit would require a power greater than 3.0 for this sortie, rather than less than 3.0 to fit the Sortie D data. It is tempting to modify this general expression with extra terms to improve the fit.

However, Figure 11 shows how well a single expression fits the data from all thirteen runs of Sorties D and E. Here the measurements are divided by the fitted values from the exponential function and the ratios are expressed in units of decibels. Over 90% of the points lie within +/- 1 dB of agreement and all points lie within +/- 4 dB. The majority of the outlying data are for the largest look angles of the last Sortie E runs.

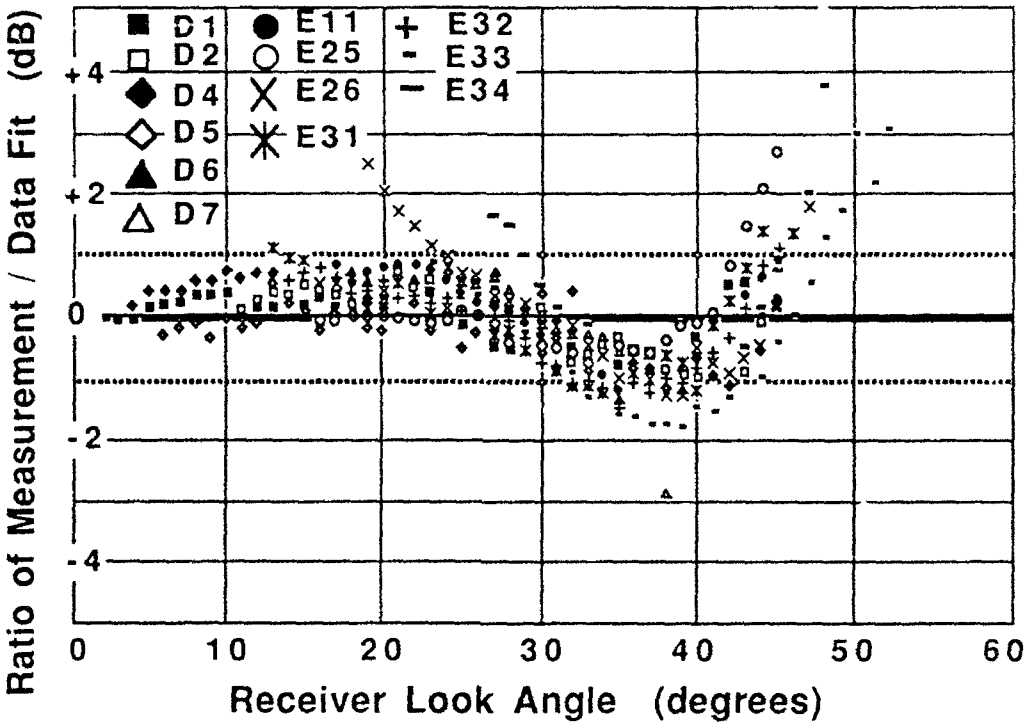

Figure 11. Cloud radiance data compared with exponential fit.

There were significant differences in visibility between Sorties D and E. In Sortie D, there apparently were foggy conditions with visibility degrading as time into the sortie increases. Received energies decreased by an order of magnitude during the runs of this sortie. Visibility changes needed to explain the received energies range from a maximum of 5.5 km at the start to a minimum of 3.8 km.

Sortie E, on the other hand, had conditions of light haze at the start and must have improved to standard clear conditions by the end. Received energies increased only slightly during the runs of this sortie. However, visibility changes needed to explain the received energies improve from a minimum of 7.0 km to a maximum of 23.5 km. At this point the optical attenuation coefficient decreases only minimally, even for very large increases of atmospheric visibility.

Figure 12 compares the exponential fit with one of the cloud models developed by Deirmendjian[1]. Karp et.al. compare this approach with that of other investigators[2]. Model outputs from Karp et.al. are shown for a blue wavelength of 0.45 μ, the infrared region of 10.6 μ, and for 1300 μ.

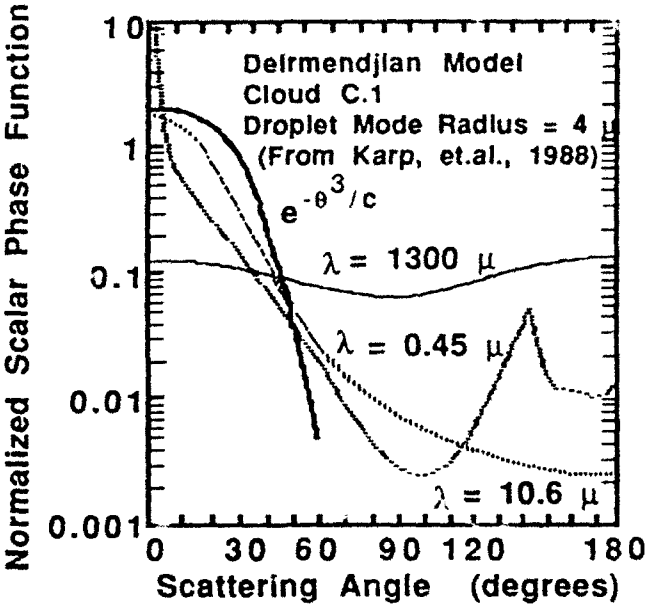

Figure 12. Deirmendjian cloud model and AOR exponential fit.

At 1300 μ, the model output is relatively flat with angle. The 10.6 μ infrared output best resembles the exponential fit for the look angle range of the measurements, 0-55°. At 0.45 μ, the model output is decidely narrower in angle and much more forward-peaked than the exponential fit.

From this plot one can see why cloud data from all runs can be fitted with a single expression. The exponential expression of the cube of the look angle is a reasonable approximation of the model's infrared output over the 0-55° look angle range for this experiment. The exponential expression fits the model's infrared prediction far better than it fits the model's blue wavelength description at 0.45 μ. This is not too upsetting.

The model's output, particularly the extent of forward peaking, depends greatly on the ratio of the typical cloud drop radius to the optical wavelength, the distribution of cloud drop sizes, and the number of particles per volume. The particular representation of clouds used in this specific model prediction is for cumulus clouds with a typical assumed scattering particle size of 4 μ.

Deirmendjian, in his discussion on natural water clouds, calls attention to California marine stratus clouds as a special case. These clouds are physically thinner than the cumulus clouds depicted in Figure 12. This is due to the fact that stratus clouds have much larger particle sizes than cumulus clouds, plus a high density of particles per volume. Thus the clouds are optically thick, even if they may be physically thin.

Deirmendjian further notes that the forward peaking shown for the plot in Figure 12 is suppressed for optical thicknesses of 16 or more, values which were exceeded for all of the cloud runs of this data set. The peaking is modeled to occur in the angle range, 0-5°, a look angle range which was not covered by cloud radiance measurements. So, it could not be proved that the forward peaking did or did not occur in this test. However, it is unlikely that this forward peaking should have occurred.

With these stratus clouds and the measured optical thicknesses, it is likely that the actual scattering function would be shaped more like the infrared curve of this plot than the visible wavelength curve.

Finally one must realize that the exponential function is a valid representation only at the small and mid-range magnitudes of look angles. At greater look angles like 80°, the distribution flattens considerably and the exponential representation becomes increasingly less valid.

5.0 CONCLUSIONS

The AOR is a very sensitive 532-nm receiver that can detect signals as weak as 1.0 E-17 J/cm^2. It was used to obtain the first significant airborne measurements of uplink laser pulses propagating through clouds at visible wavelengths. Most of this work was done with a laser submerged at a water depth of 30 m, comparable to 2.5 scattering lengths, and through 300 m of optically thick clouds. This has provided several major results.

First, is that it has been shown that these data can be explained by conventional scattering physics and through existing propagation models. The received energy and pulse width data were well-behaved from: pulse-to-pulse, run-to-run and night-to-night. The consistency in propagation physics that was observed builds confidence in the use of models for describing optical uplink propagation.

Second, the measured radiance pattern of the uplink laser was significantly narrower than modeled or expected for both clouds and hazes. The radiance pattern has a dramatic roll-off in signal energy at look angles of 35-40°, rather than the 60° angle that had been expected for these patterns. Previous experiements had lacked the system sensitivity and tracking capability to sample this roll-off with look angle.

Third, all of the measured cloud radiance profiles could be described by a single mathematical expression as

$$E = E_o\, e^{-\theta^3 / 35{,}000} \text{ ; Cloud Radiance Profile}$$

This expression agrees well with a Deirmendjian cloud model for receiver look angles of 0-55°. This simple expression may not be valid for look angles greater than this. However, cloud radiance profiles for stratus and cumulus clouds are significantly narrower in look angle space than the cosine-shaped profile used in some uplink models. The marine stratus clouds observed during this test may have significantly different properties than marine cumulus clouds and stratus clouds in the open ocean, well away from coastal influences.

Fourth, the energy in laser spots on the tops of clouds is distributed in the horizontal plane like a Gaussian function, as modeled. Spot size, however, was much larger than modeled, resulting in more spreading loss (greater than a factor of five) than predicted. Test conditions were outside the value ranges of the cloud model[4].

Fifth, haze and light fog can play a major part in the link equation for optical propagation. During this test the uplink radiance profile out of the water was completely masked by the effects of a haze. The measured profile can be well-described by

$$E = E_o\, e^{-\theta/21^\circ} \text{ ; Haze Radiance Profile}$$

The haze pattern is explained, qualitatively and quantitatively, by Mie scattering theory and compares well with Deirmendjian's continental haze model[1,2]. This simple expression can be used for look angles of 0-90° for hazes. We had severely underestimated the signal spreading and attenuation effects of hazes and fogs on uplink optical propagation. Additional information on the spatial and temporal occurrences of these effects is needed. Visibility measurements in future experiments should be a requirement.

Sixth, it would have been better to measure the cloud physical and optical thicknesses during each sortie, including a measurement of the particle size distributions in clouds and hazes. The differences between these observations and the cited models can be explained by different particle size distributions. Gathering these data is difficult to do with one aircraft, but a ship-mounted LIDAR system with complementary use of instrumented balloons or rockets could address most of the measurement needs.

6. REFERENCES

1. D. Deirmendjian, *Electromagnetic Scattering on Spherical Polydispersion* , Elsevier, New York, 1969.
2. S. Karp, R.M. Gagliardi, S.E. Moran and L.B. Stotts, *Optical Channels: Fibers, Clouds, Water and the Atmosphere.*, Plenum Press, New York, 1988.
3. R. Lintell and M. Groves, "Ocean Field Test Data Analysis", SAIC Report (Unpublished), 1989.
4. Titan Systems, Inc., "Satellite Laser Communications Evaluation Algorithm (SLCEVAL) - Version 5 Supplemental Reports (U)", NOSC Technical Document 1634, 1989.